IEEE Access
Multidisciplinary : Rapid Review : Open Access Journal

Received 27 May 2024, accepted 2 July 2024, date of publication 8 July 2024, date of current version 16 July 2024.

Digital Object Identifier 10.1109/ACCESS.2024.3424695

RESEARCH ARTICLE

A New Chaotic System With Two Stable Node-Foci Equilibria and an Unstable Saddle-Focus Equilibrium: Bifurcation and Multistability Analysis, Circuit Design, Voice Cryptosystem Application, and FPGA Implementation

TALAL BONNY[1], SUNDARAPANDIAN VAIDYANATHAN[2,3], WAFAA AL NASSAN[1], FAREH HANNACHI[4], AND ACENG SAMBAS[5,6]

[1]Department of Computer Engineering, University of Sharjah, Sharjah, United Arab Emirates
[2]Centre for Control Systems, Vel Tech University, Chennai, Tamil Nadu 600062, India
[3]Centre of Excellence for Research, Value Innovation and Entrepreneurship (CERVIE), UCSI University, Cheras, Kuala Lumpur 56000, Malaysia
[4]Department of Management Sciences, Echahid Cheikh Larbi Tebessi University, Tebessa 12002, Algeria
[5]Faculty of Informatics and Computing, Universiti Sultan Zainal Abidin, Terengganu 21300, Malaysia
[6]Department of Mechanical Engineering, Universitas Muhammadiyah Tasikmalaya, Tasikmalaya 46196, Indonesia

Corresponding author: Talal Bonny (tbonny@sharjah.ac.ae)

ABSTRACT In the recent years, significant research interest has been devoted in the modelling and applications of chaotic systems with stable equilibria. In this research study, we propose a new 3-D chaotic system with two stable node-foci equilibria and an unstable saddle-focus equilibrium. We conduct a detailed bifurcation analysis for the new chaotic system with the aid of bifurcation diagrams and Lyapunov exponents. We also show that the new chaotic system has multistability with coexisting attractors. Using MultiSim version 14.1, we design an electronic circuit for the proposed 3-D chaotic system. Finally, as an application, we introduce a voice cryptosystem using the new chaotic system with two stable node-foci equilibrium points and an unstable saddle-focus equilibrium point and its hardware realization on the FPGA platform.

INDEX TERMS Bifurcation, chaos, chaotic systems, circuits, equilibrium, FPGA.

I. INTRODUCTION

Chaos theory deals with the modelling, analysis and applications of chaotic dynamical systems which are highly sensitive to changes in the initial states of the systems [1]. Chaotic systems have several applications in engineering such as cryptography ([2], [3]), robotics ([4], [5]), neural networks ([6], [7]), mechanical systems ([8], [9]), secure communications ([10], [11]), memristive systems ([12], [13], [14], [15]), cryptosystems [16], etc.

In the recent years, significant interest has been shown in the chaos literature in the modelling of chaotic dynamical systems with stable equilibria ([17], [18], [19], [20], [21]). Yang et al. [17] proposed a quadratic chaotic system consisting of two stable node-foci equilibria. Yang et al. [18] proposed a multi-wing chaotic system with two or more stable node-foci equilibria. Johansyah et al. [19] announced a new financial risk system with one stable equilibrium and

The associate editor coordinating the review of this manuscript and approving it for publication was Binit Lukose.

two unstable equilibria. Vaidyanathan et al. [20] described the finding of a new 3-D chaotic jerk system with a stable equilibrium. Ahmad et al. [21] reported the finding of stable equilibria and hidden chaotic attractors for the smooth cubic Chua's circuit.

Data encryption is essential to guarantee the information security of the transferred data [22], [23]. Numerous cryptography standards and protocols have been proposed to address information security concerns, such as the Advanced Encryption Standard (AES), the Data Encryption Standard (DES), the Triple Data Encryption Standard (3DES), and the RSA algorithm. While every popular encryption technique has pros and cons, these cryptographic techniques do not deal with the distribution of encryption keys. To overcome this limitation, recent studies used chaotic systems in cryptography since the chaotic signal is aperiodic, broadband, and has a large spectrum to conceal the message inside [24], [25].

In literature, the realization of cryptogram-based chaotic systems was demonstrated using a variety of methods, including analog circuits and digital circuits that use digital signal processors (DSP) and Field Programmable Gate Array (FPGA) [26], [27], [28].

In this research work, we obtain a new 3-D chaotic system with two stable node-foci equilibrium points and an unstable saddle-focus equilibrium point by adding a linear term to the third differential equation of the Yang et al. chaotic system [17] and considering a different set of parameter values. The maximal Lyapunov exponent (MLE) of a 3-D chaotic system is the positive Lyapunov exponent of the system, which pinpoints the chaotic behavior of the system [29].

In our work, we establish that the new chaotic system has a greater value of MLE than that of the Yang et al. chaotic system [17]. We also show that the Kaplan-Yorke dimension of the new chaotic system is greater than that of the Yang chaotic system [17]. We also give a detailed bifurcation analysis of the new chaotic system with the aid of bifurcation diagrams and Lyapunov exponents.

In the chaos literature, there is special interest shown in developing chaotic systems with stable equilibrium points as such systems possess hidden attractors and they have many engineering applications [30]. The proposed chaotic system has the special property of one unstable equilibrium and two stable equilibrium points. Hence, the proposed chaotic system exhibits hidden attractors.

Circuit design of chaotic systems aids in the real-world engineering applications of the chaotic systems ([31], [32], [33]). In this research study, we build an electronic design of the proposed 3-D chaotic system with two stable node-foci equilibria and an unstable saddle-focus equilibrium using MultiSim 14.1.

As an application, we introduce a voice cryptosystem using the new chaotic system with two stable node-foci equilibrium points and an unstable saddle-focus equilibrium point and hardware realization of the FPGA platform.

II. A NEW CHAOTIC SYSTEM WITH TWO STABLE NODE-FOCI AND ONE UNSTABLE SADDLE-FOCUS EQUILIBRIUM POINTS

In 2010, Yang et al. [17] proposed a new chaotic system with two quadratic nonlinear terms given by:

$$\begin{cases} \dot{x} = a(y-x) \\ \dot{y} = -ky - xz \\ \dot{z} = -b + xy \end{cases} \tag{1}$$

We assume that in the system (1), $X = (x, y, z)$ represents the state and a, b, k are real parameters that take positive values. Yang et al. [17] showed that the system (1) exhibits chaotic motion with two stable node-foci equilibrium points for the parameter values $(a, b, k) = (10, 100, 11.2)$. It is easy to check that the Yang system (1) has rotation symmetry about the z-axis.

For numerical simulations, we take the parameter values as $a = 10, b = 100, k = 11.2$ and the initial state of the Yang system (1) as $x(0) = 0.9, y(0) = 1.8$ and $z(0) = 0.5$. Then the Lyapunov exponents of the Yang system (1) were calculated using MATLAB as $L_1 = 0.8437, L_2 = 0$ and $L_3 = -22.0433$. Also, we observe the Kaplan dimension of the Yang system (1) as

$$D_K = 2 + \frac{L_1 + L_2}{|L_3|} = 2.0383 \tag{2}$$

The equilibrium points of the Yang system (1) are obtained by setting $\dot{x} = \dot{y} = \dot{z} = 0$. Thus, we solve the following equations:

$$a(y-x) = 0 \tag{3a}$$

$$-ky - xz = 0 \tag{3b}$$

$$-b + xy = 0 \tag{3c}$$

From (3a), we get $x = y$. Then the equations (3b) and (3c) can be simplified as follows:

$$-x(z+k) = 0 \tag{4a}$$

$$x^2 - b = 0 \tag{4b}$$

From (4a), either $x = 0$ or $z = -k$. The solution $x = 0$ is inadmissible since it contradicts (4b). Thus, we must have $z = -k$. From (4b), we get $x = \sqrt{b}$. Hence, the Yang system (1) has two equilibrium points given by $P_1 = (\sqrt{b}, \sqrt{b}, -k)$ and $P_2 = (-\sqrt{b}, -\sqrt{b}, -k)$

For the chaotic case given by $(a, b, k) = (10, 100, 11.2)$, the equilibrium points of the Yang system (1) are: $P_1 = (10, 10, -11.2)$ and $P_2 = (-10, -10, -11.2)$ The eigenvalues of the linearization matrix of the Yang system (1) at P_1 and P_2 are found to be equal and given by

$$\lambda_1 = -20.9778, \lambda_{2,3} = -0.1111 \pm 9.7635\, i \tag{5}$$

This shows that the equilibrium points P_1 and P_2 of the Yang chaotic system (1) are stable node-foci. Hence, the Yang system (1) exhibits hidden attractors.

TABLE 1. Kaplan Dimension and Lyapunov Exponents for the Yang system (1) and the proposed chaotic system (6).

Chaotic System	Lyapunov exponents			MLE	Kaplan dimension
	L_1	L_2	L_3		
Yang system [17]	0.8437	0	−22.0433	0.8437	2.0383
New system	1.0768	0	−32.8764	1.0768	2.0451

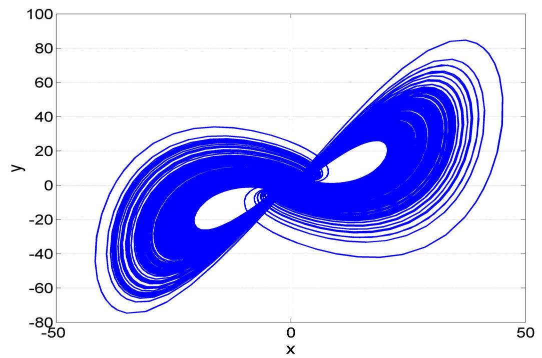

FIGURE 1. Phase plot of the two-scroll attractor of the system (6) in (x, y)- plane.

In this research work, we obtain a new 3-D chaotic system with two stable node-foci equilibrium points and an unstable saddle-focus equilibrium point by adding a linear term to the third differential equation of the Yang system (1) and considering a different set of parameter values.

We propose a new 3-D nonlinear system with two quadratic nonlinear terms given by the dynamics

$$\begin{cases} \dot{x} = a(y-x) \\ \dot{y} = -ky - xz \\ \dot{z} = -b + xy + pz \end{cases} \tag{6}$$

We assume that in the new system (6), $X = (x, y, z)$ represents the state and a, b, k, p are real parameters that take positive values. We shall establish in this research work that the new system (6) exhibits chaotic motion with two stable node-foci equilibrium points and one unstable saddle-focus equilibrium point for the parameter values $(a, b, k, p) = (11, 145, 12, 0.2)$.

It is easy to check that the new system (6) has rotation symmetry about the z-axis.

For numerical simulations, we take the parameter values of (6) as $a = 11, b = 145, k = 12$, and $p = 0.2$. we take the initial state of (6) as $x(0) = 0.9, y(0) = 1.8$ and $z(0) = 0.5$.

Then the Lyapunov exponents of the new chaotic system (6) were calculated using MATLAB as $L_1 = 1.0768, L_2 = 0$ and $L_3 = -23.8764$. Also, we observe the Kaplan dimension of the new chaotic system (6) as

$$D_K = 2 + \frac{L_1 + L_2}{|L_3|} = 2.0451 \tag{7}$$

Table 1 shows that the proposed chaotic system (6) has more complexity than the Yang chaotic system (1).

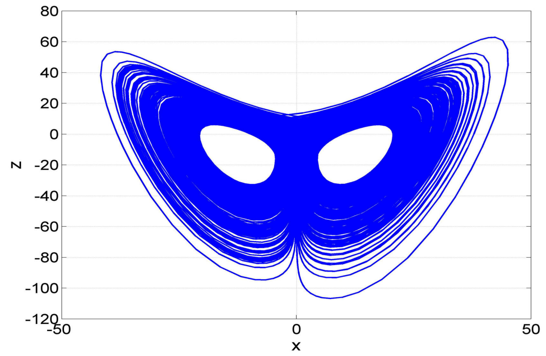

FIGURE 2. Phase plot of the two-scroll attractor of the system (6) in (x, z)- plane.

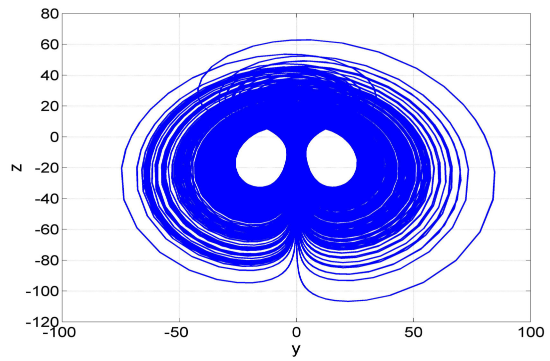

FIGURE 3. Phase plot of the two-scroll attractor of the system (6) in (y, z)- plane.

Next, we calculate the equilibrium points of the new system (6) and analyze their stability properties.

The equilibrium points of the new chaotic system (6) are obtained by setting $\dot{x} = \dot{y} = \dot{z} = 0$. Thus, we solve the following equations:

$$a(y-x) = 0 \tag{8a}$$

$$-ky - xz = 0 \tag{8b}$$

$$-b + xy + pz = 0 \tag{8c}$$

From (8a), we get $x = y$. Then the equations (8b) and (8c) can be simplified as follows:

$$-x(z+k) = 0 \tag{9a}$$

$$-b + x^2 + pz = 0 \tag{9b}$$

We have two cases to consider, viz. Case (A): $x = 0$, and Case (B): $x \neq 0$.

First, we consider Case (A), i.e. we assume that $x = 0$. Since $x = y$, we must have $y = 0$. Substituting $x = 0$ in (9b), we get $pz = b$ or $z = b/p$.

In Case (A), the new system (6) has the equilibrium $Q_0 = (0, 0, b/p)$, which is on the z-axis.

Next, we consider Case (B), i.e. we assume that $x \neq 0$. From (9a), we have $z = -k$. Then Eq. (9b) can be simplified as$x^2 = b + pk$ or $x = \sqrt{b + pk}$.

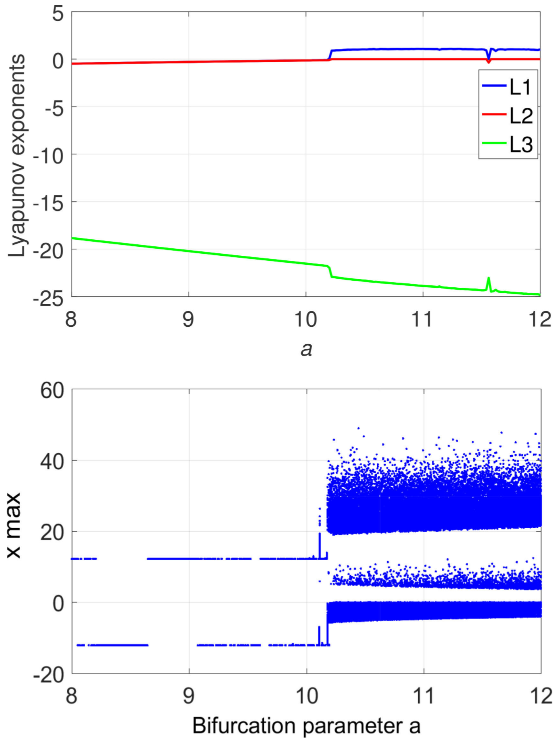

FIGURE 4. Lyapunov exponents spectrum and bifurcation diagram of the system (6) for $a \in [8, 12]$.

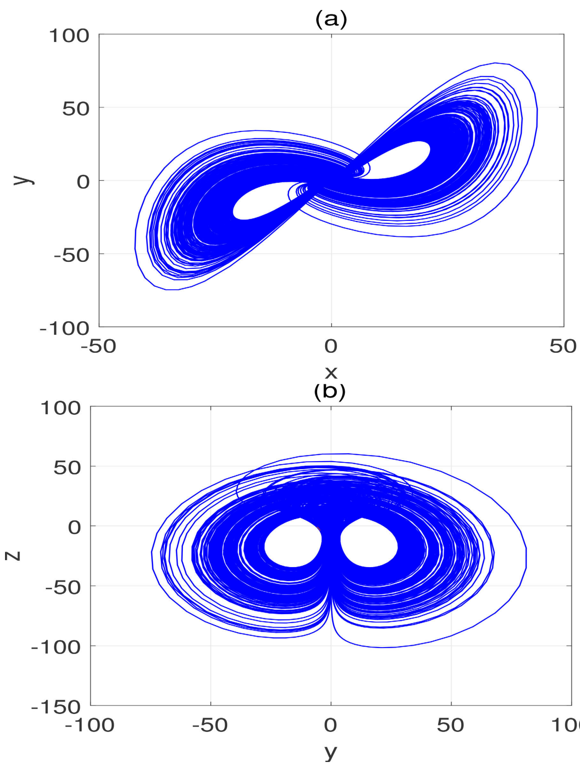

FIGURE 5. Chaotic behaviours of the system (6) when $b = 145$, $k = 12$, and $p = 0.2$: (a) chaotic for $a = 11.5$, (b) chaotic for $a = 12$.

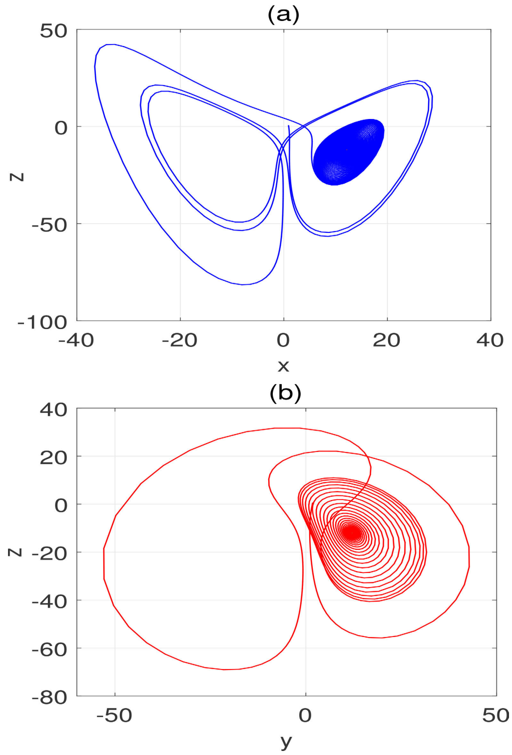

FIGURE 6. Behaviours of the system (6) when $b = 145$, $k = 12$, and $p = 0.2$: (a) converges to the equilibrium for $a = 10$, (b) converges to the equilibrium for $a = 9$.

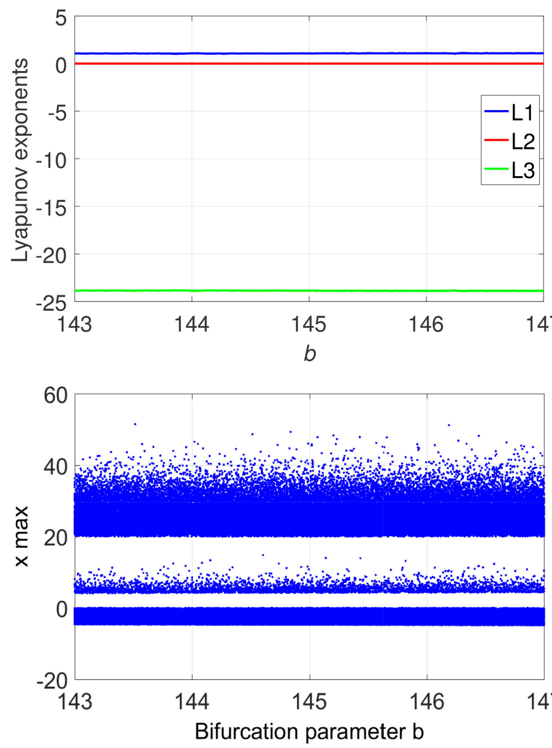

FIGURE 7. Lyapunov exponents spectrum and bifurcation diagram of the system (6) for $b \in [143, 147]$.

In Case (B), the new system (6) has two equilibrium points given by $Q_1 = (\sqrt{b+pk}, \sqrt{b+pk}, -k)$ and $Q_2 = (-\sqrt{b+pk}, -\sqrt{b+pk}, -k)$. In the chaotic case, the parameter values are taken as $(a, b, k, p) = (11, 145, 12, 0.2)$. In this case, the equilibrium points of

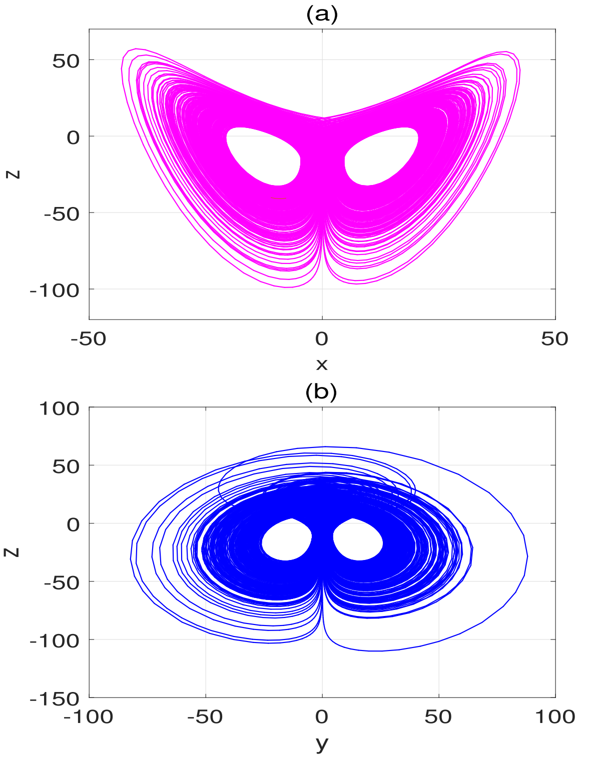

FIGURE 8. **Chaotic behaviour of the system (6) when $a = 11$, $k = 12$, and $p = 0.2$: (a) chaotic for $b = 144$, (b) chaotic for $b = 146$.**

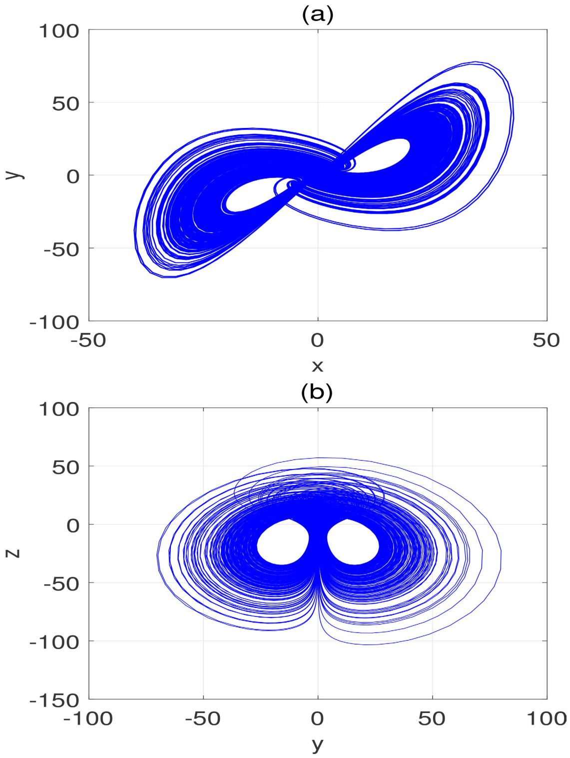

FIGURE 10. **Chaotic behaviours of the system (6) when $a = 11$, $b = 145$ and $p = 0.2$: (a) chaotic for $k = 11$, (b) chaotic for $k = 13$.**

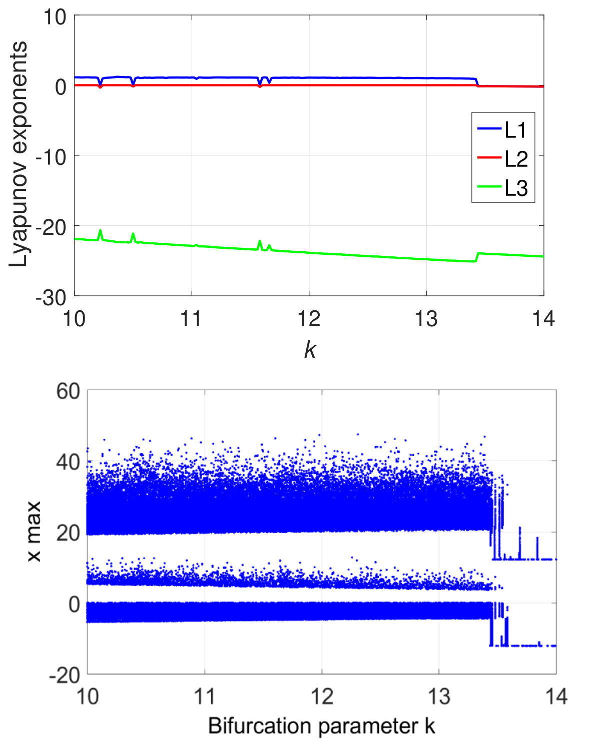

FIGURE 9. **Lyapunov exponents spectrum and bifurcation diagram of the system (6) for $k \in [10, 14]$.**

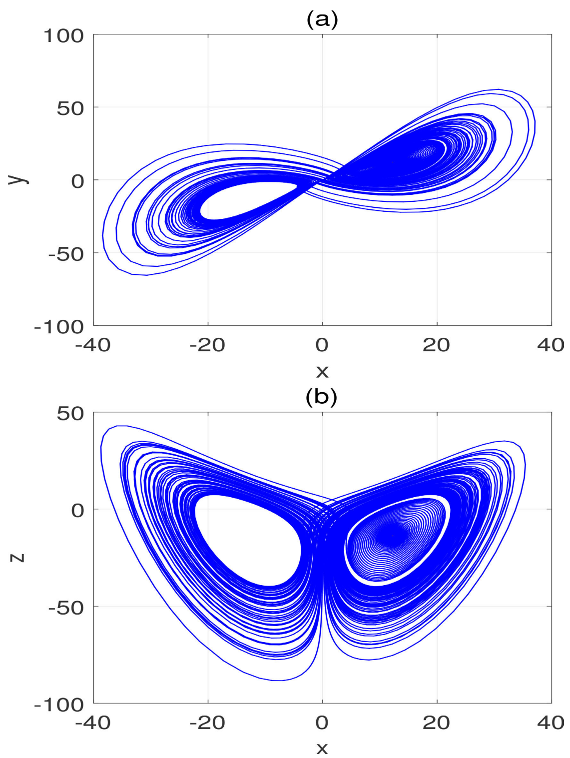

FIGURE 11. **Behaviours of the system (6) when $a = 11$, $b = 145$, and $p = 0.2$: (a) converges to the equilibrium for $k = 13.5$, (b) converges to the equilibrium for $k = 13.84$.**

the new system (6) are obtained as $Q_0 = (0, 0, 725)$ and $Q_1 = (12.1408, 12.1408, -12)$ and $Q_2 = (-12.1408, -12.1408, -12)$ The eigenvalues of the linearization matrix of the new system (6) at Q_0 are found

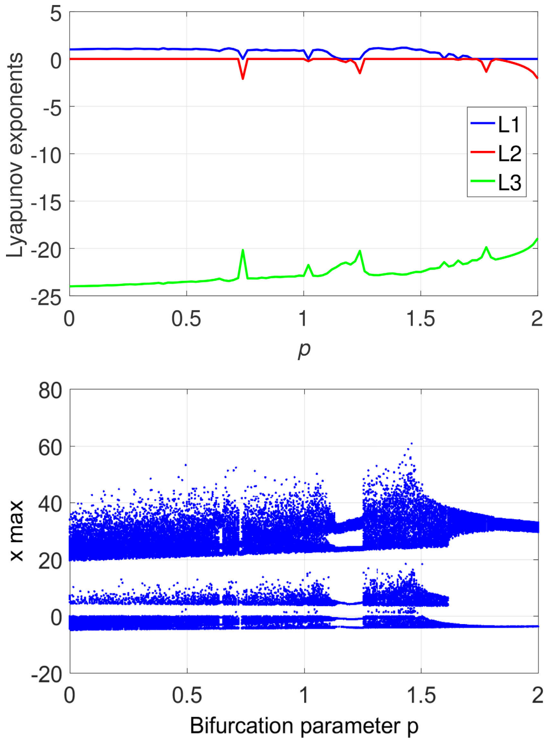

FIGURE 12. Lyapunov exponents spectrum and bifurcation diagram of the system (6) for $p \in [0, 2]$.

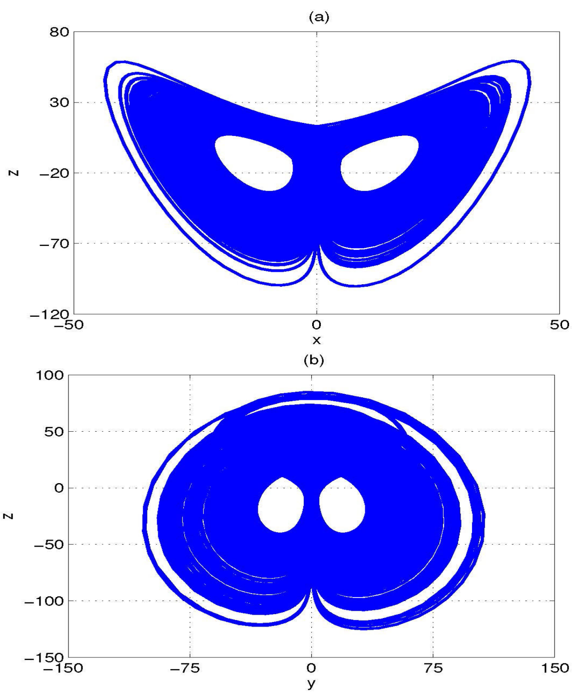

FIGURE 13. Behaviours of system (6) when $a = 11$, $b = 145$, and $k = 12$: (a) chaotic for $p = 0.4$, (b) chaotic for $p = 1.4$.

as follows:

$$\lambda_1 = 0.2, \lambda_{2,3} = -11.5 \pm 89.3015i \tag{10}$$

This calculation shows that Q_0 is an unstable saddle-focus equilibrium point. The eigenvalues of the linearization matrix

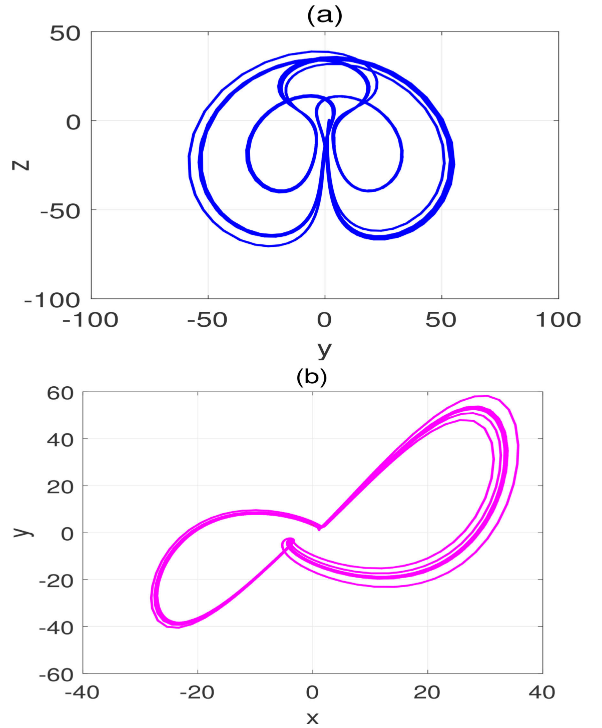

FIGURE 14. Behaviours of system (6) when $a = 11$, $b = 145$, and $k = 12$: (a) periodic for $p = 1.2$, (b) periodic for $p = 1.9$.

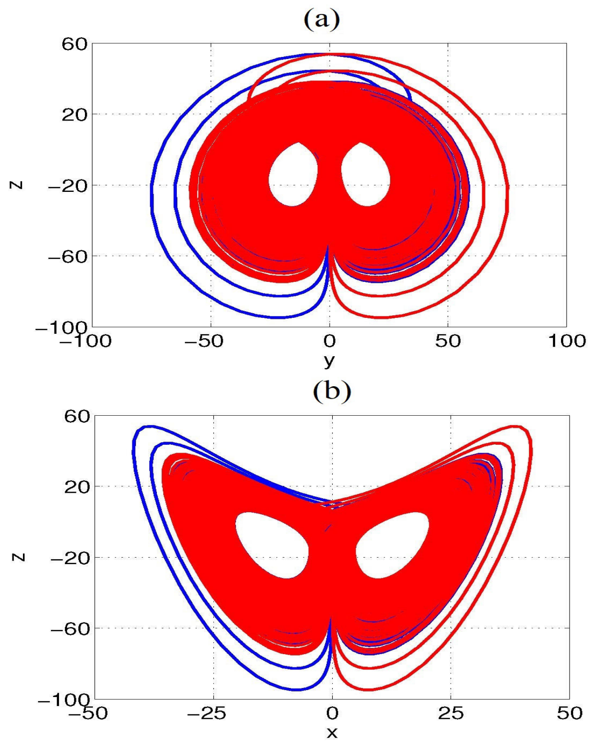

FIGURE 15. Coexistence of two attractors for parameters: $a = 12$, $b = 145$, $k = 12$, $p = 0.2$ with different initial values: The blue orbit for $(1, 5, 4)$ and the red orbit for $(-1, -5, 4)$.

of the new system (6) at Q_1 and Q_2 are found to be equal and they are given as follows:

$$\lambda_1 = -22.7803, \lambda_{2,3} = -0.0099 \pm 11.9311i \tag{11}$$

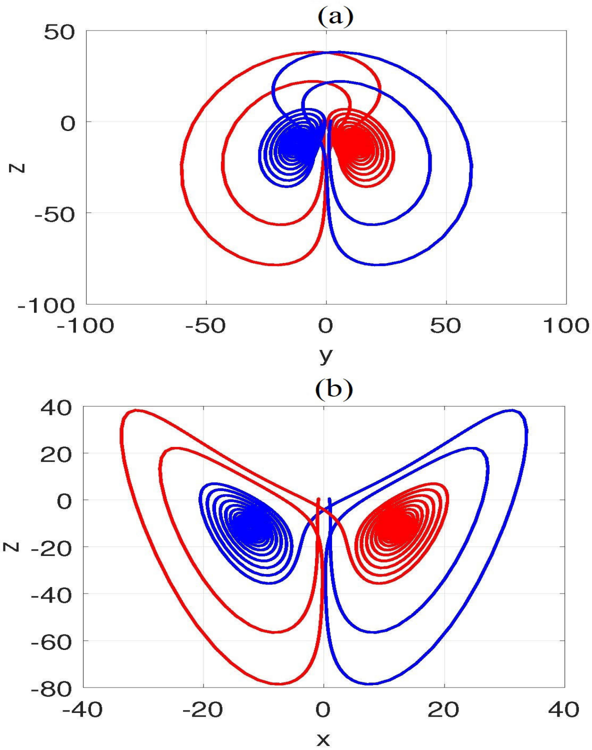

FIGURE 16. Coexistence of two attractors for parameters: $a = 8.5, b = 145, k = 12, p = 0.2$ with different initial values: The blue orbit for (0.9, 1.8, 0.5) and the red orbit for (−0.9, −1.8, 0.5).

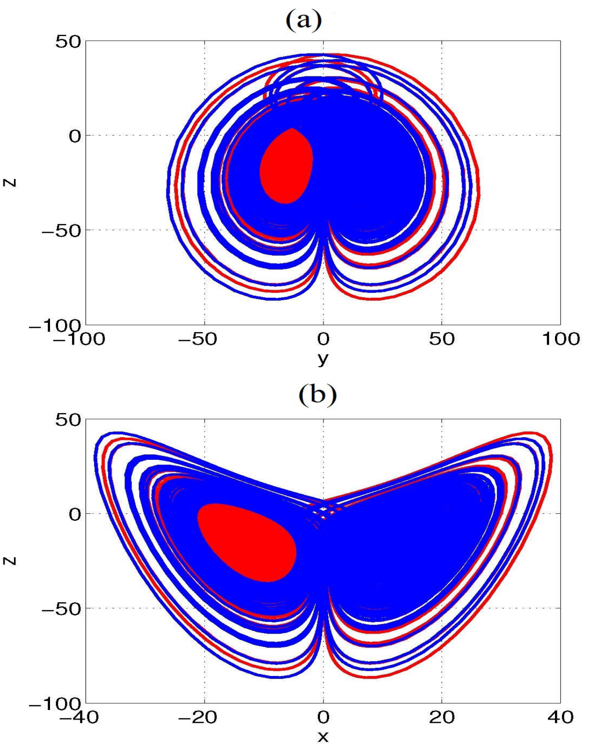

FIGURE 17. Coexistence of two attractors for parameters: $a = 11, b = 145, k = 13.5, p = 0.2$ with different initial values: The blue orbit for (0.9, 1.8, 0.5) and the red orbit for (−0.9, −1.8, 0.5).

This calculation shows that the equilibrium points Q_1 and Q_2 of the new chaotic system (6) are stable node-foci. Hence, the new chaotic system (6) exhibits hidden attractors.

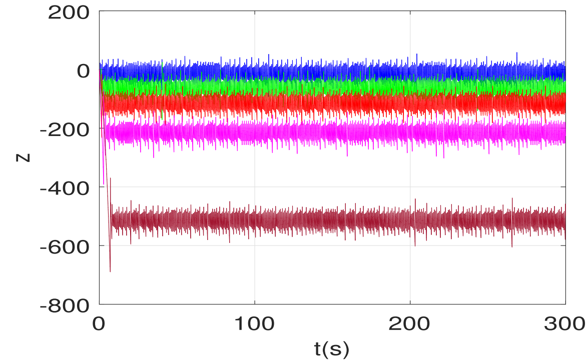

FIGURE 18. The signal z with different values of the offset boosting controller m: for: $m = 0$ (blue colour);$m = 50$ (green colour) $m = 100$ (red colour); $m = 200$ (magenta colour);$m = 500$ (brown colour).

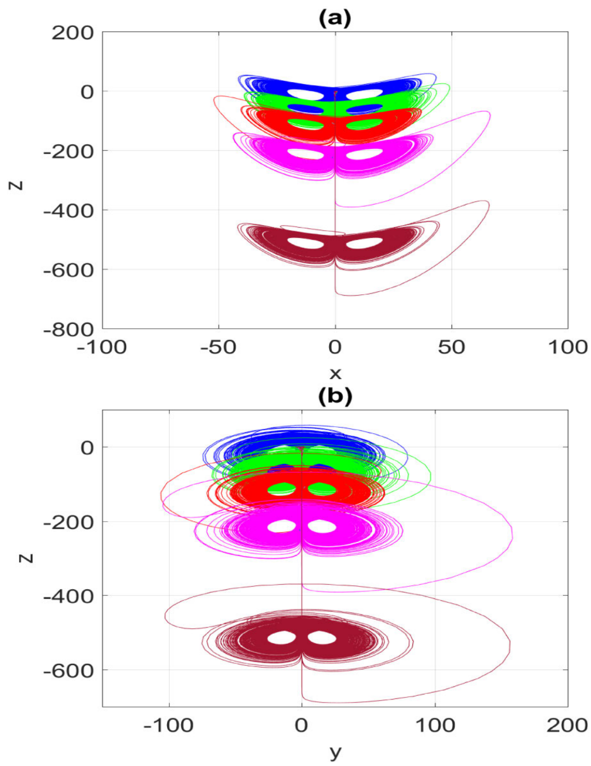

FIGURE 19. Phase portraits in different planes and different values of the offset boosting controller m: (a) $x - z$ plane, (b) $y - z$ plane for: $m = 0$ (blue colour);$m = 50$ (green colour) $m = 100$ (red colour);$m = 200$ (magenta colour);$m = 500$ (brown colour).

Figures 1-3 show the MATLAB signal plots of the two-scroll chaotic attractor of the new chaotic system (6) for the parameter values taken as $a = 11, b = 145, k = 12, p = 0.2$ and the initial state taken as $x(0) = 0.9, y(0) = 1.8$ and $z(0) = 0.5$.

III. BIFURCATION ANALYSIS OF THE NEW TWO-SCROLL SYSTEM

In this section, we investigate numerically the dynamical behaviors of the new chaotic system (6) using the Lyapunov

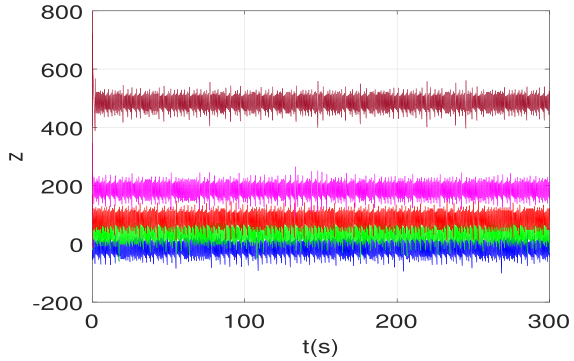

FIGURE 20. The signal z with different values of the offset boosting controller m: for: $m = 0$ (blue colour);$m = -50$ (green colour) $m = -100$ (red colour);$m = -200$ (magenta colour);$m = -500$ (brown colour).

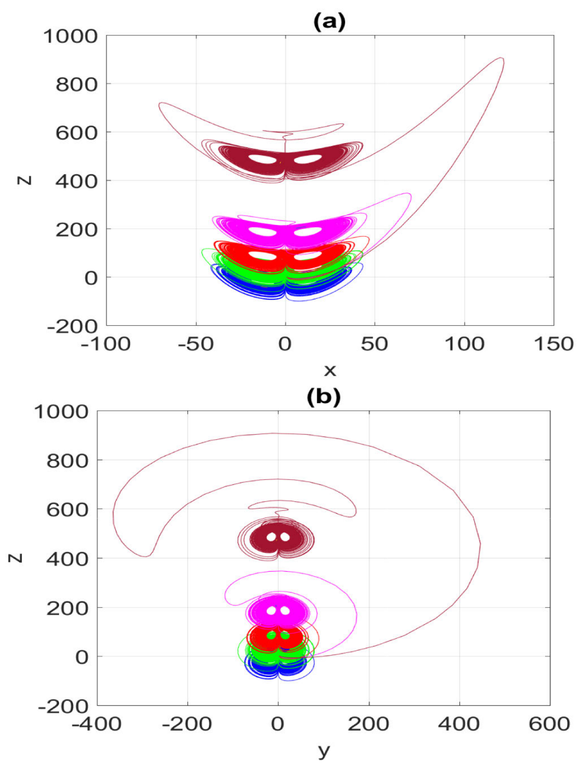

FIGURE 21. Phase portraits in different planes and different values of the offset boosting controller m: (a) $x - z$ plane, (b) $y - z$ plane for: $m = 0$ (blue colour);$m = -50$ (green colour) $m = -100$ (red colour);$m = -200$ (magenta colour);$m = -500$ (brown colour).

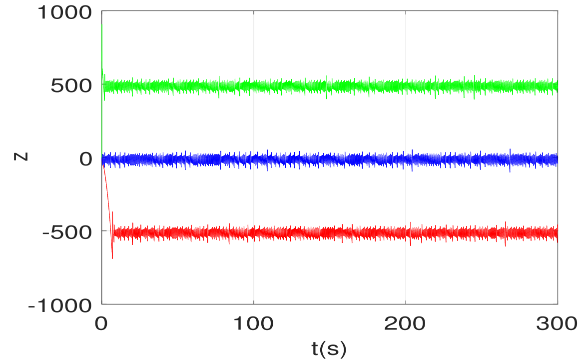

FIGURE 22. The signal z with different values of the offset boosting controller m: $m = 0$ (blue colour);$m = 500$ (red colour);$m = -500$ (green colour).

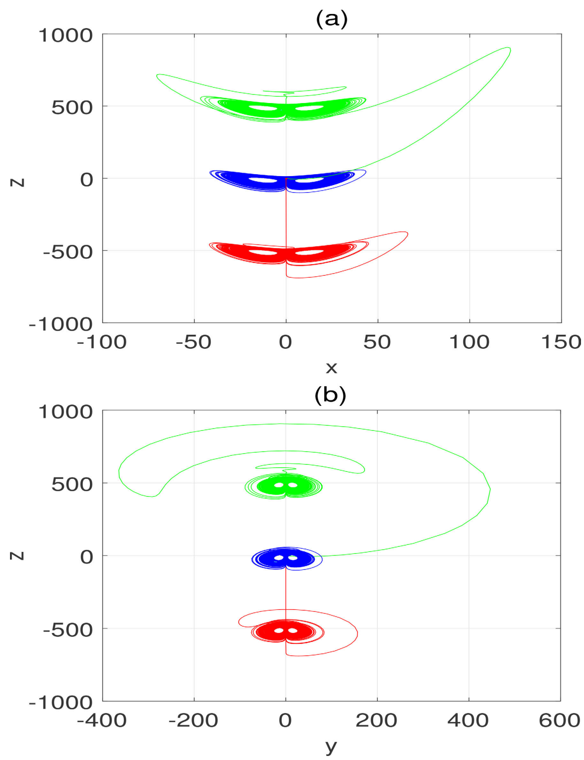

FIGURE 23. Phase portraits in different planes and different values of the offset boosting controller m: (a) $x - z$ plane, (b) $y - z$ plane for: $m = 0$ (blue colour);$m = 500$ (red colour);$m = -500$ (green colour).

exponents spectrum and bifurcation diagrams. Figures 4-12 show the Lyapunov exponents spectrum and the bifurcations diagrams of system (6) with respect to parameter a, b, k, p respectively. Obviously, when $a \in [8, 12]$, $b \in [143, 147]$, $k \in [10, 14]$, and $p \in [0, 2]$ the behaivour of the system (6) is either chaotic, periodic or converge to an equilibria. We carry out the bifurcation analysis of the new two-scroll system (6) with respect to each parameter in the following subsections.

A. VARIATION OF THE PARAMETER a

We can identify the behavior of the system (6) when the parameter a varies in the range [8, 12] as follows:

we fix the values of the parameters as $b = 145$, $k = 12$, $p = 0.2$ and Let $a \in [4, 5]$ and define:

$$A = [10.2, 12]$$
$$B = [0, 10.2]$$

When $a \in B$, it can be seen from Fig. 4, the system (6) has three negative Lyapunov exponent ($L_{1,2,3} < 0$). Thus the system (6) converges to an equilibrum point in this range of the parameter a.

The values of Lyapunov exponents when $a = 8.5$ are computed as

$$L_1 = -0.3831, \quad L_2 = -0.385, \quad L_3 = -19.53$$

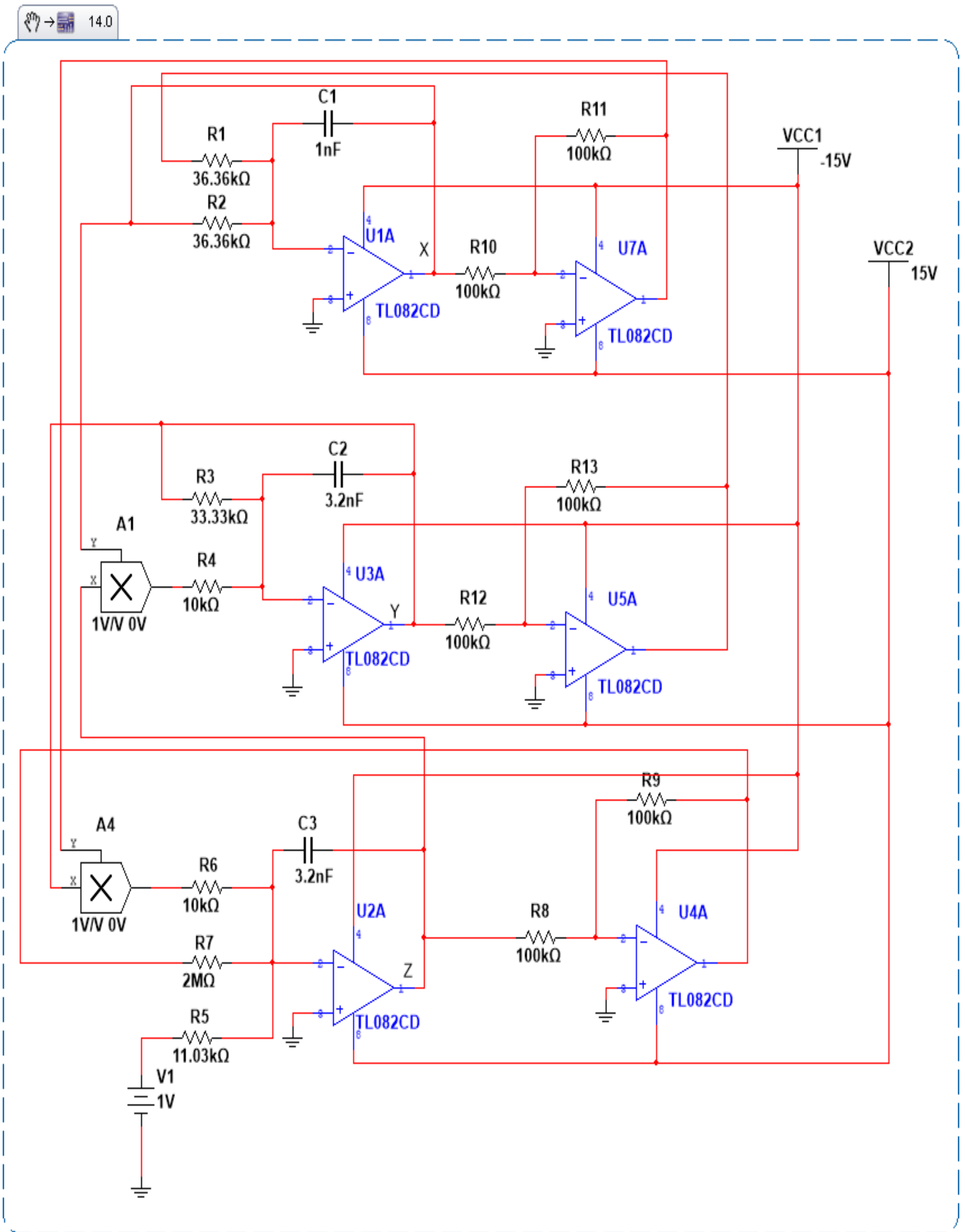

FIGURE 24. Electronic circuit of the new chaotic system using MultiSIM 14.0.

The values of Lyapunov exponents when $a = 9$ are computed as

$$L_1 = -0.2936, \quad L_2 = -0.2961, \quad L_3 = -20.21$$

Also, the values of Lyapunov exponents when $a = 10$ are computed as

$$L_1 = -0.1356, \quad L_2 = -0.1402, \quad L_3 = -21.52$$

When $a \in A$, it can be seen from Fig. 4 that the system (6) has $L_1 > 0$, $L_2 = 0$ and $L_3 < 0$.

Thus, the system (6) is chaotic and generates a chaotic attractor.

The values of Lyapunov exponents when $a = 10.5$ are computed as

$$L_1 = 1.024, \quad L_2 = 0, \quad L_3 = -23.32$$

The values of Lyapunov exponents when $a = 11.5$ are computed as

$$L_1 = 1.077, \quad L_2 = 0, \quad L_3 = -23.88$$

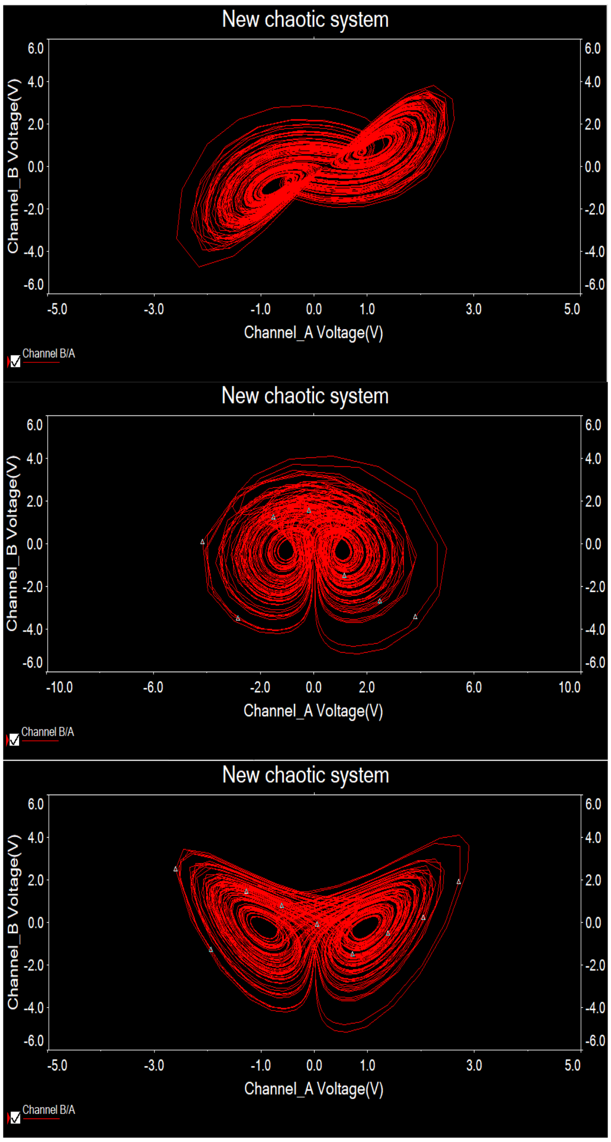

FIGURE 25. **Chaotic attractor of new chaotic system using MultiSIM 14.0.**

Also, the values of Lyapunov exponents when $a = 12$ are computed as

$$L_1 = 1.023, \quad L_2 = 0, \quad L_3 = -24.82$$

Figures 5 and 6 show the behaviours of the system (6) for different values of the parameter a, while the other parameters are fixed as $b = 145$, $k = 12$ and $p = 0.2$.

B. VARIATION OF THE PARAMETER b

When we fix the values of the parameters as $a = 11$, $k = 12$, $p = 0.2$ and Let $b \in [143, 147]$, it can be seen from Fig. 7, that the system (6) has $L_1 > 0$, $L_2 = 0$ and $L_3 < 0$. Thus, the system (6) is chaotic and generates a chaotic attractor.

The values of Lyapunov exponents when $b = 144$ are computed as

$$L_1 = 1.078, \quad L_2 = 0, \quad L_3 = -23.88$$

The values of Lyapunov exponents when $b = 146$ are computed as

$$L_1 = 1.088, \quad L_2 = 0, \quad L_3 = -23.89$$

Figure 8 shows the chaotic behaviour of the system (6) for different values of b, when the other parameters are fixed as $a = 11$, $k = 12$, and $p = 0.2$.

C. VARIATION OF THE PARAMETER k

We can identify the behavior of the system (6) when the parameter k varies in the range [10, 14] as follows:

In this case, when $k \in [10, 13.4371324]$, it can be seen from Fig. 9, that the system (6) has $L_1 > 0$, $L_2 = 0$ and $L_3 < 0$. Thus, the system (6) is chaotic and generates a chaotic attractor.

The values of Lyapunov exponents when $k = 11$ are computed as

$$L_1 = 1.09, \quad L_2 = 0, \quad L_3 = -22.89$$

The values of Lyapunov exponents when $k = 12.5$ are computed as

$$L_1 = 1.058, \quad L_2 = 0, \quad L_3 = -24.36$$

Also, the values of Lyapunov exponents when $k = 13$ are computed as

$$L_1 = 0.9986, \quad L_2 = 0, \quad L_3 = -24.36$$

When $k \in [13.4371326, 14]$, it can be seen from Fig. 9, that the system (6) has three negative Lyapunov exponents ($L_{1,2,3} < 0$). Thus the system (6) converges to an equilibrium point in this range of parameter k.

The values of Lyapunov exponents when $k = 13.5$ are computed as

$$L_1 = -0.1352, \quad L_2 = -0.1522, \quad L_3 = -24.01$$

Also, the values of Lyapunov exponents when $k = 13.84$ are computed as

$$L_1 = -0.1777, \quad L_2 = -0.1835, \quad L_3 = -24.28$$

Figures 10 and 11 show the various behaviours of the system (6) for different values of k, when the other parameters are fixed as $a = 11$, $b = 145$ and $p = 0.2$.

D. VARIATION OF THE PARAMETER p

When $p \in [0, 1.16[\cup]1.24, 1.72[$, it can be seen from Fig.12, that the system (6) has $L_1 > 0$, $L_2 = 0$ and $L_3 < 0$. Thus, the system (6) is chaotic and generates a chaotic attractor.

The values of Lyapunov exponents when $p = 0.4$ are computed as

$$L_1 = 1.134, \quad L_2 = 0, \quad L_3 = -23.73$$

Also, the values of Lyapunov exponents when $p = 1.4$ are computed as

$$L_1 = 1.118, \quad L_2 = 0, \quad L_3 = -22.72$$

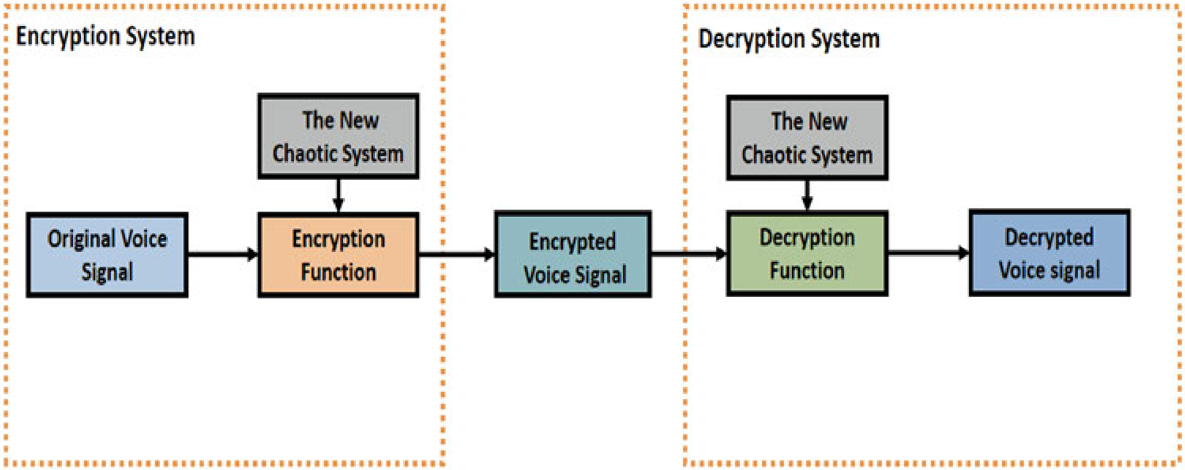

FIGURE 26. The proposed voice encryption systems.

When $p \in [1.16, 1.24] \cup [1.72, 2]$, it can be seen from Fig. 12, that it has one zeo Lyapunov exponent ($L_1 = 0$) and two negative Lyapunov exponents ($L_{2,3} < 0$). Thus the system (6) is periodic in this range of the parameter p.

The values of Lyapunov exponents when $p = 1.2$ are computed as

$$L_1 = 0, \quad L_2 = -0.039581, \quad L_3 = -21.70$$

Also, the values of Lyapunov exponents when $p = 1.9$ are computed as

$$L_1 = 0, \quad L_2 = -0.4558, \quad L_3 = -20.64$$

Figures 13 and 14 show the various behaviours of the system (6) for different values of p, when the other parameters are fixed as $a = 11$, $b = 145$ and $k = 12$.

A summary of the bifurcation analysis of the new chaotic system (6) is provided in Table 2.

IV. MULTISTABILITY IN THE NEW CHAOTIC SYSTEM

In order to study the coexistence attractors and other characteristics of the system better, it is necessary to give some disturbance to the initial conditions under the condition of keeping the system parameters constant.

The new chaotic system (6) is invariant under the change of coordinates

$$(x, y, z) \longrightarrow (-x, -y, z) \tag{12}$$

This shows that the new system (6) has rotation symmetry about the z-axis. Figures 15-17 show the dynamic behavior with coexistence chaotic attractors with different initial conditions.

V. OFFSET BOOSTING

In this section, we will discuss the offset boosting control. Adding a constant ''m'' to a variable in a nonlinear system will produce an offset. Obviously, the state of the system (6) can be controllable and the offset-boosted system is obtained from system (6) by replacing *VARIABLE* with *VARIABLE* + m in the equations of the system (6) as follows:

Case: for z variabale The system (13) can be controllable and the offset-boosted system is obtained from the system (6) by replacing z with $z + m$ in the equations of the system (6) as follows:

$$\begin{cases} \dot{x} = a(y - x) \\ \dot{y} = -ky - x(z + m) \\ \dot{z} = -b + xy + p(z + m) \end{cases} \tag{13}$$

Consequently, when increasing or deceasing the boosting controller m, It can be seen from figures 18,20, and 22 that the chaotic signal z can be boosted from a bipolar signal to a unipolar one. The Phase portraits in different planes and different values of the offset boosting controller m are given in Figures 19, 21, and 23.

VI. CIRCUIT DESIGN OF THE NEW CHAOTIC SYSTEM

Several studies indicate that ordinary differential equations can be represented through electronic circuits. However, designing a circuit directly based on system equations may result in abnormal functioning. To address this, an operational-amplifier approach is employed to scale down the variables' states of the new chaotic system (6) and achieve strange attractors. In accordance with system equations, the scaling variables X, Y and Z are defined as $X = \frac{1}{4}x$, $Y = \frac{1}{4}y$,and $Z = \frac{1}{4}z$, where x, y and z are the state variables of the new system. This system can be practically realized using common electronic components such as resistors, capacitors, analog multipliers, and operational amplifiers. The rescaled chaotic system is given as follow:

$$\begin{cases} \dot{X} = a(Y - X) \\ \dot{Y} = -kY - 4XZ \\ \dot{Z} = -\dfrac{b}{4} + 4XY + pZ \end{cases} \tag{14}$$

TABLE 2. A Summary of the Bifurcation Analysis of the New Chaotic System (6).

Dynamical Behavior	Parameter a	Parameter b	Parameter k	Parameter p	L_1	L_2	L_3
Stable Equilibrium	9	145	12	0.2	-0.29356	-0.29614	-20.21029
Stable Equilibrium	10	145	12	0.2	-0.13561	-0.14015	-21.52423
Stable Equilibrium	11	145	13.5	0.2	-0.13523	-0.15218	-24.01259
Stable Equilibrium	11	145	13.84	0.2	-0.17880	-0.18346	-24.27773
Chaotic Attractor	11.5	145	12	0.2	1.03327	0	-24.33263
Chaotic Attractor	12	145	12	0.2	1.02297	0	-24.82259
Chaotic Attractor	11	145	12	0.2	1.07837	0	-23.87763
Chaotic Attractor	11	145	12	0.2	1.08811	0	-23.88715
Chaotic Attractor	11	145	11	0.2	1.09030	0	-22.88950
Chaotic Attractor	11	145	13	0.2	0.99856	0	-24.79795
Chaotic Attractor	11	145	12	0.4	1.13377	0	-23.73318
Chaotic Attractor	11	145	12	1.4	1.11786	0	-22.71688
Periodic Orbit	11	145	12	1.2	0	-0.09580	-21.70474
Periodic Orbit	11	145	12	1.9	0	-0.45576	-20.64463

The electronic circuit for implementing the new chaotic system is synthesized, as depicted in Fig. 24. The equations governing the circuit are formulated as follows:

$$\begin{cases} C_1\dot{X} = \dfrac{1}{R_1}Y - \dfrac{1}{R_2}X \\ C_2\dot{Y} = -\dfrac{1}{R_3}Y - \dfrac{1}{10R_4}XZ \\ C_3\dot{Z} = -\dfrac{1}{R_5}V_1 + \dfrac{1}{10R_6}XY + \dfrac{1}{R_7}Z \end{cases} \tag{15}$$

Here, *x, y, z*, and *w* are the output voltages of the operational amplifiers U1A, U2A, and U3A, respectively. The values of circuit components are selected as: $R_1 = R_2 = 36.36\ \mathrm{k\Omega}$, $R_3 = 33.33\ \mathrm{k\Omega}$, $R_4 = R_6 = 10\ \mathrm{k\Omega}$, $R_5 = 11.03\ \mathrm{k\Omega}$, $R_7 = 2\ \mathrm{M\Omega}$, $R_8 = R_9 = R_{10} = R_{11} = R_{12} = R_{13} = 100\ \mathrm{k\Omega}$, $C_1 = C_2 = C_3 = 3.2$ nF.

The phase portraits of the system (6) are visually depicted in Fig. 25 through oscilloscope graphics. It is evident that the circuit simulation results of the oscilloscope graphics presented in Fig. 25 align with the MATLAB simulation results provided in Fig.24.

VII. VOICE CRYPTOSYSTEM USING THE NEW CHAOTIC OSCILLATOR

This section demonstrates the scheme for a voice cryptosystem using the new 3-D chaotic system with two stable node-foci equilibrium points and an unstable saddle-focus equilibrium point in (6).

Figure 26 illustrates the block diagram of the proposed cryptosystem, which uses the new chaotic system as a key generator. It is worth mentioning that in a chaos-based cryptosystem, ensuring the synchronization between the chaotic systems on both the encryption and decryption sides is essential to decrypt the voice signal successfully. In this paper, we align both chaotic systems with identical initial conditions. Thus, the decrypted voice signal corresponds precisely to the original input.

As in Figure 26, the encryption function obtains the encryption process, which employs the random sequence generated by the new chaotic system to scramble the original voice signal. At the beginning of the encryption process, it is worth mentioning that the state variables generated by the chaotic system need to be normalized to match the amplitude of the voice signal. Then, the voice signal $V(t)$ and the normalized chaotic states variables xn(t), yn(t), and zn(t) are combined, producing the encrypted voice signal $E(t)$.

The integration between the key generated by the chaotic system and the voice signal generates a sophisticated signal with the chaotic system's randomness and unpredictability characteristics. In our system, the encryption function is described as follows:

$$E(t) = V(t) + x_n(t) + y_n(t) + z_n(t) \tag{16}$$

Here $V(t)$ is the original voice signal, $E(t)$ is the encrypted signal and $x_n(t), y_n(t), z_n n(t)$ are the normalized state variables generated by the new chaotic system.

The decryption function involves the inverse function to recover the original voice signal. The decryption function subtracts the normalized chaotic state variables from the received encrypted signal, producing the decrypted signal D(t). In our system, the decryption function is described as follows:

$$D(t) = E(t) - (x_n(t) + y_n(t) + z_n(t)) \tag{17}$$

Assuming that the chaotic systems used in the encryption and decryption systems are synchronized and have the same initial conditions, then the decrypted voice signal matches the original voice signal.

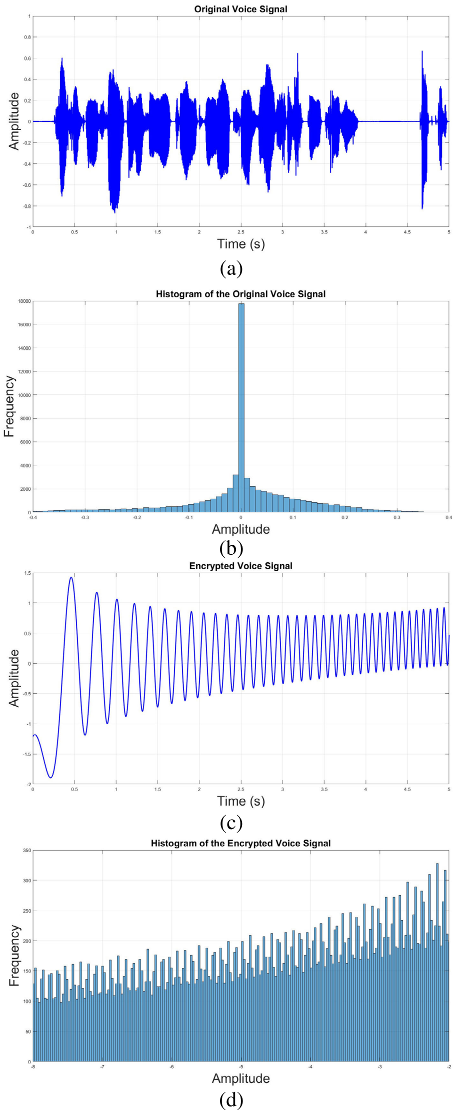

FIGURE 27. (a) The waveform of the original voice signal, (b) The histogram of the original voice signal, (c) The waveform of the encrypted voice signal, and (d) The histogram of the encrypted voice signal.

Figure 27 displays the waveforms and the corresponding histograms for the original and encrypted voice signals. The method transforms the original voice into an encrypted voice that is completely different. Moreover, the histogram of the original signal has a normal distribution and could be detected by statistical attacks. However, the distribution of the encrypted signal is flat and can hide its features as much as possible.

Correlation Coefficient (CC), Signal Noise Ratio (SNR), and Percentage Residual Deviation (PRD) tests are applied to evaluate the resistance of the proposed system against statistical attacks. Table 3 displays the values that were computed for various voice signals.

The correlation between adjacent encrypted signal samples is one method of assessing the efficacy of encryption systems.

TABLE 3. Correlation coefficient, SNR, and PRD between the original and encrypted audio files.

Voice Signal	CC	SNR	PRD
Signal-1	0.0008	-48.3487	2.6148e+04
Signal-2	0.0003	-49.8652	3.1136e+04
Signal-3	0.0006	-49.8718	3.1159e+04
Signal-4	0.0003	-51.1147	3.5953e+04

FIGURE 28. Fixed point representation of the variables in the voice cryptosystem.

The small, obtained value of the (CC) shows that the encrypted signal is random.

Signal-to-noise ratio (SNR) is one of the most used objective metrics for assessing the original audio signal's strength. The highly negative SNR readings in Table 3 suggest that the encrypted voice signals are outstanding.

The Percentage Residual Deviation (PRD)One statistical method to determine how much the encrypted voice signal differs from the original signal. Table 3 provides the computed percent residual deviation values for original and encrypted audio streams.

Hence, the proposed system makes the signal more difficult for an attacker to use the encrypted data to derive partial sample information.

VIII. FPGA IMPLEMENTATION OF THE VOICE CRYPTOSYSTEM

This section describes the implementation of the proposed voice cryptosystem using FPGA (Field Programmable Gate Array). The FPGAs play a vital role in the hardware implementation of different systems due to their characteristics, such as parallel processing and real-time response. The proposed voice cryptosystem consists of two separate systems: the encryption system and the decryption system. The hardware implementation of both the encryption and decryption systems are performed using the VHDL code. Where each system is realized on the FPGA Cyclon V platform using QUARTUS software. We use the 32-bit fixed-point arithmetic representation for all the variables and constants for the FPGA implementation. This representation has 1-bit for the sign, 10-bits for the integer part, and 21-bits for the fractional part as in Figure 28.

Figure 29 shows the top-level entity of the encryption system, consisting of four inputs: clock, reset, initial conditions, and the voice signal and one output represents the encrypted voice signal.

The detailed block diagram of the encryption system is shown in Figure 30, which consists of two subsystems: the new chaotic system and the encryption function.

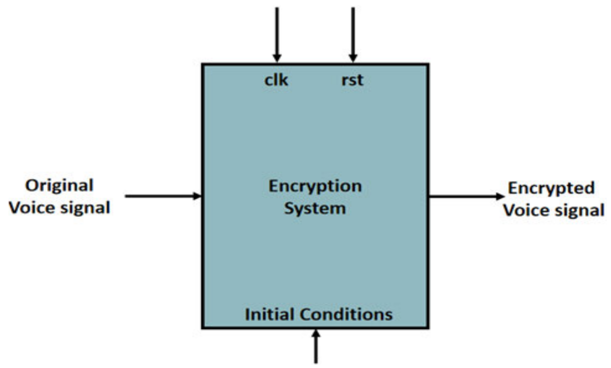

FIGURE 29. Top-level entity of the encryption system.

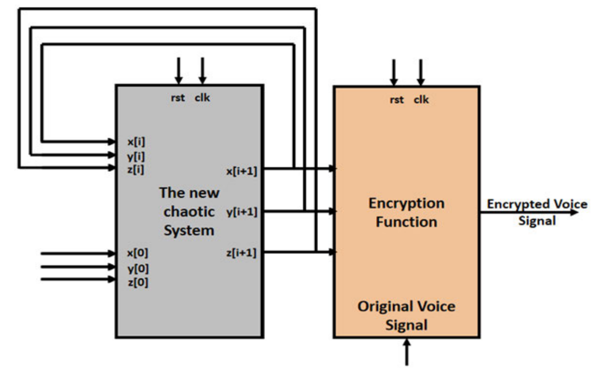

FIGURE 30. The detailed block diagram of encryption system.

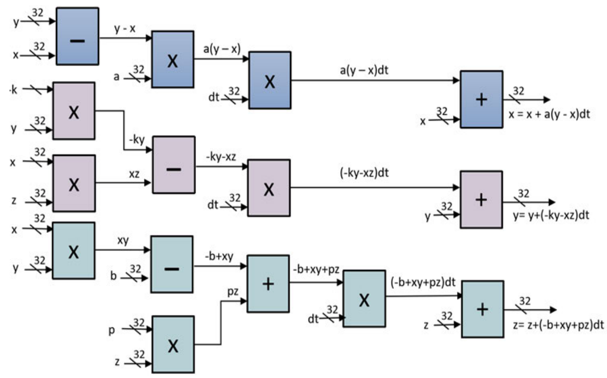

FIGURE 31. Basic blocks connections to implement the state variables x,y, and z of the new chaotic system.

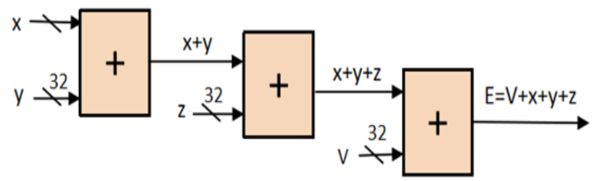

FIGURE 32. Basic blocks connections to implement the encryption function block.

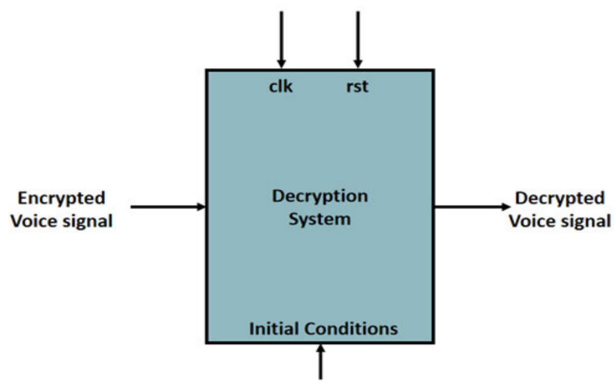

FIGURE 33. Top-level entity of the decryption system.

The new chaotic system generates the chaotic sequence that is used to encrypt the voice signal. To implement the new chaotic system on FPGA, we apply the forward Euler integration method on the mathematical representation of the new chaotic system given in the equations (6) as follows:

$$
\begin{aligned}
x[i+1] &= x[k] + (a(y[i] - x[i]))dt \\
y[i+1] &= y[k] + (-ky[i] - x[i]z[i])dt \\
z[i+1] &= z[k] + (-b + x[i]y[i] + pz[i])dt
\end{aligned} \tag{18}
$$

Here i and $i+1$ represent the current and the next states, respectively, and dt represents the discretization step. The VHDL entity that represents the new chaotic system in Figure 30 consisting of a clock, reset, and three inputs representing the current state variables $x[i], y[i], z[i]$, three inputs represent the initial conditions $x[0], y[0], z[0]$, and three outputs representing the future state variables x[i + 1], y[i + 1], $z[i+1]$. At the beginning, the initial conditions $x[0], y[0]$, and $z[0]$ define the starting values of the state variables. Then, the outputs are fed back to the inputs to generate a chaotic sequence to calculate the future values. The new chaotic system block is built based on the discrete Equations (18). The detailed block diagram of the new chaotic system consists of three subsystems one for each of the state variables x, y, and z as shown in Figure 31.

Finally, Figure 32 illustrates the basic blocks that represents the encryption function block in Figure 29. The encryption function block takes the outputs of the new chaotic system $x[i+1]$, $y[i+1]$, $z[i+1]$ as encryption key and apply Equation (16) to obtain the encrypted voice signal.

The top-level entity of the decryption system is depicted in Figure 33. It comprises of four inputs: clock, reset, initial conditions, and the encrypted voice signal. The output, on the other hand, depicts the decrypted voice signal.

The detailed block diagram of the decryption system is shown in Figure 34, which consists of two subsystems: the new chaotic system and the decryption function. Where the new chaotic system is similar to the chaotic system in the encryption system shown in Figure 31. The detailed block diagram of the decryption function block is shown in Figure 35. The decryption function performs a mathematical equation (17) to recover the original signal after considering

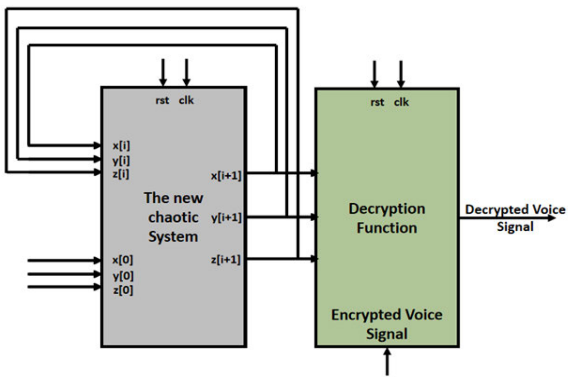

FIGURE 34. The detailed block diagram of the decryption system.

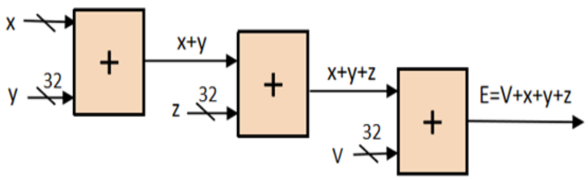

FIGURE 35. Basic blocks connections to implement the decryption function block.

TABLE 4. FPGA resources utilization for the communication system.

Resources	Encryption System		Decryption System	
	Units	Utilization	Units	Utilization
Logic Utilization	2203	7 %	2204	7 %
Total Registers	212	–	212	–
Total Pins	162	7 %	162	7 %
Maximum Frequency (MHz)	33.38	–	33.42	–

the outputs of the new chaotic system, $x[i+1]$, $y[i+1]$, and $z[i+1]$, as the decryption key.

Table 4 illustrates the FPGA resource utilization for implementing the proposed voice cryptosystem for the encryption and decryption systems. The Encryption system utilizes 2203 logic units (7% of available logic), 212 registers, and 162 pins (7% of total). Its maximum operating frequency is 33.38 MHz. Similarly, the decryption system for the logic units, registers, and pins, with a matching frequency of 33.42 MHz.

IX. COMPARISON RESULTS FOR THE NEW VOICE ENCRYPTION SYSTEM

In this section, the new encryption system is compared to the current algorithms. In this comparison, various quality metrics used, such as Correlation Coefficient (CC), Signal Noise Ratio (SNR), and Percentage Residual Deviation (PRD) are tabulated in Table 5. By comparing the obtained metrics using our proposed system with those of the previous encryption systems shown in Table 5, we may evaluate the proposed system's performance increase in comparison to current approaches. The suggested system performs competitively or better than previous research works in this area.

TABLE 5. Performance metrics comparison of the proposed encryption scheme with other methods.

Encryption Algorithm	CC	SNR	PRD
[34]	-0.001	–	–
[35]	0.001466	-15.38255	–
[36]	-0.0004282	-25.4968	–
[37]	0.0189	-22.1621	–
Proposed system	0.0003	-51.1147	3.5953e+04

Based on the results of the security analysis and the comparison with related work, our proposed system has a high security level making it a practical option for the application of voice encryption. However, this system has some deficiencies that need to be considered. One significant challenge that faces our system is related to the synchronization between the chaotic systems. Although our methodology assumed the synchronization between the chaotic systems in both the encryption and the decryption sides, we understand the need to provide an illustration of the synchronization procedure. Additionally, the implementation of the voice cryptosystem, along with synchronization, is associated with complexity related to hardware and computational resources.

X. CONCLUSION

There is significant research interest in the chaos literature in the mathematical modelling and applications of chaotic systems with stable equilibria. The main contribution of this research work is the modelling of a new 3-D chaotic system with two stable node-foci equilibria and an unstable saddle-focus equilibrium. We performed a detailed bifurcation analysis for the new chaotic system with the aid of bifurcation diagrams and Lyapunov exponents. We also showed that the new chaotic system has multistability with coexisting attractors. Using MultiSim version 14.1, we designed an electronic circuit for the proposed 3-D chaotic system. Finally, as an engineering application, we had introduced a voice cryptosystem using the new chaotic system with two stable node-foci equilibrium points and an unstable saddle-focus equilibrium point and hardware realization of the FPGA platform. We illustrated our results with many simulations.

REFERENCES

[1] F. C. Moon, *Chaotic and Fractal Dynamics: Introduction for Applied Scientists and Engineers*, 2nd ed., Weinheim, Germany: Wiley-VCH, 1992.

[2] L. Du, L. Teng, H. Liu, and H. Lu, "Multiple face images encryption based on a new non-adjacent dynamic coupled mapping lattice," *Exp. Syst. Appl.*, vol. 238, Mar. 2024, Art. no. 121728.

[3] H. Zhu, J. Ge, J. He, and L. Zhang, "A non-degenerate chaotic bits XOR system with application in image encryption," *Math. Comput. Simul.*, vol. 219, pp. 231–250, May 2024.

[4] S. G. Khan, "Adaptive chaos control of a humanoid robot arm: A fault-tolerant scheme," *Mech. Sci.*, vol. 14, no. 1, pp. 209–222, Apr. 2023.

[5] E. Petavratzis, C. Volos, and I. Stouboulos, "Experimental study of terrain coverage of an autonomous chaotic mobile robot," *Integration*, vol. 90, pp. 104–114, May 2023.

[6] S. Asif, M. Zhao, Y. Li, F. Tang, and Y. Zhu, "CGO-ensemble: Chaos game optimization algorithm-based fusion of deep neural networks for accurate mpox detection," *Neural Netw.*, vol. 173, May 2024, Art. no. 106183.
[7] N. Anwar, I. Ahmad, A. K. Kiani, M. Shoaib, and M. A. Z. Raja, "Novel intelligent predictive networks for analysis of chaos in stochastic differential SIS epidemic model with vaccination impact," *Math. Comput. Simul.*, vol. 219, pp. 251–283, May 2024.
[8] A. Ding, S. Hu, and L. Zhou, "Chaotic dynamics of a duffing oscillator subjected to external and nonlinear parametric excitations with delayed feedbacks," *J. Comput. Nonlinear Dyn.*, vol. 19, no. 4, Apr. 2024, Art. no. 041003.
[9] D. Costa, E. Pavlovskaia, and M. Wiercigroch, "Feedback control of chaos in impact oscillator with multiple time-delays," *Chaos, Solitons Fractals*, vol. 181, Apr. 2024, Art. no. 114570.
[10] N. Charalampidis, A. Iatropoulos, and C. Volos, "Chaos based speech encryption using microcontroller," *Integration*, vol. 95, Mar. 2024, Art. no. 102128.
[11] Z. Li, H. Wang, and Y. Ji, "Hardware fingerprint construction of optical transmitters based on permutation entropy spectrum of chaos for secure authentication," *Opt. Laser Technol.*, vol. 171, Apr. 2024, Art. no. 109947.
[12] Q. Lai, L. Yang, and G. Chen, "Design and performance analysis of discrete memristive hyperchaotic systems with stuffed cube attractors and ultraboosting behaviors," *IEEE Trans. Ind. Electron.*, vol. 71, no. 7, pp. 7819–7828, Jul. 2024.
[13] Q. Lai, Z. Wan, and P. D. K. Kuate, "Generating grid multi-scroll attractors in memristive neural networks," *IEEE Trans. Circuits Syst. I, Reg. Papers*, vol. 70, no. 3, pp. 1324–1336, Mar. 2023.
[14] Q. Lai, Z. Wan, H. Zhang, and G. Chen, "Design and analysis of multiscroll memristive Hopfield neural network with adjustable memductance and application to image encryption," *IEEE Trans. Neural Netw. Learn. Syst.*, vol. 34, no. 10, pp. 7824–7837, Oct. 2023, doi: 10.1109/TNNLS.2022.3146570.
[15] Q. Lai and Z. Chen, "Dynamical analysis and finite-time synchronization of grid-scroll memristive chaotic system without equilibrium," *Chaos, Solitons Fractals*, vol. 176, Nov. 2023, Art. no. 114118.
[16] Q. Lai and Y. Liu, "A cross-channel color image encryption algorithm using two-dimensional hyperchaotic map," *Exp. Syst. Appl.*, vol. 223, Aug. 2023, Art. no. 119923.
[17] Q. Yang, Z. Wei, and G. Chen, "An unusual 3D autonomous quadratic chaotic system with two stable node-FOCI," *Int. J. Bifurcation Chaos*, vol. 20, no. 4, pp. 1061–1083, Apr. 2010.
[18] Y. Yang, L. Huang, N. V. Kuznetsov, B. Chai, and Q. Guo, "Generating multiwing hidden chaotic attractors with only stable node-foci: Analysis, implementation and application," *IEEE Trans. Ind. Electron.*, vol. 71, no. 4, pp. 3986–3995, Apr. 2024, doi: 10.1109/TIE.2023.3273242.
[19] M. D. Johansyah, A. Sambas, S. Zheng, K. Benkouider, S. Vaidyanathan, M. A. Mohamed, and M. Mamat, "A novel financial system with one stable and two unstable equilibrium points: Dynamics, coexisting attractors, complexity analysis and synchronization using integral sliding mode control," *Chaos, Solitons Fractals*, vol. 177, Dec. 2023, Art. no. 114283.
[20] S. Vaidyanathan, A. T. Azar, I. A. Hameed, K. Benkouider, E. Tlelo-Cuautle, B. Ovilla-Martinez, C.-H. Lien, and A. Sambas, "Bifurcation analysis, synchronization and FPGA implementation of a new 3-D jerk system with a stable equilibrium," *Mathematics*, vol. 11, no. 12, p. 2623, Jun. 2023.
[21] I. Ahmad, B. Srisuchinwong, and M. U. Jamil, "Coexistence of hidden attractors in the smooth cubic Chua's circuit with two stable equilibria," *Int. J. Bifurcation Chaos*, vol. 33, no. 4, Mar. 2023, Art. no. 2330010.
[22] T. Bonny, W. A. Nassan, and A. Baba, "Voice encryption using a unified hyper-chaotic system," *Multimedia Tools Appl.*, vol. 82, no. 1, pp. 1067–1085, Jan. 2023.
[23] F. AlMutairi and T. Bonny, "Image encryption based on Chua chaotic oscillator," in *Proc. 3rd Int. Conf. Signal Process. Inf. Secur. (ICSPIS)*, Nov. 2020, pp. 1–4.
[24] W. A. Nassan, T. Bonny, K. Obaideen, and A. A. Hammal, "AN LSTM model-based prediction of chaotic system: Analyzing the impact of training dataset precision on the performance," in *Proc. Int. Conf. Electr. Comput. Technol. Appl. (ICECTA)*, Nov. 2022, pp. 337–342.
[25] F. Al Mutairi and T. Bonny, "New image encryption algorithm based on switching-type chaotic oscillator," in *Proc. Int. Conf. Electr. Comput. Technol. Appl. (ICECTA)*, Nov. 2019, pp. 1–5.
[26] M. AlFarah and T. Bonny, "Chaotic oscillator prediction based on artificial neural network and its realization on FPGA," in *Proc. Adv. Sci. Eng. Technol. Int. Conferences (ASET)*, Feb. 2022, pp. 1–4.
[27] T. Bonny and A. Haq, "Emulation of high-performance correlation-based quantum clustering algorithm for two-dimensional data on FPGA," *Quantum Inf. Process.*, vol. 19, no. 6, p. 179, Jun. 2020.
[28] T. Bonny and J. Henkel, "Huffman-based code compression techniques for embedded processors," *ACM Trans. Design Autom. Electron. Syst.*, vol. 15, no. 4, pp. 1–37, Sep. 2010.
[29] A. Wolf, J. B. Swift, H. L. Swinney, and J. A. Vastano, "Determining Lyapunov exponents from a time series," *Phys. D, Nonlinear Phenomena*, vol. 16, no. 3, pp. 285–317, Jul. 1985.
[30] V.-T. Pham, S. Vaidyanathan, C. Volos, and T. Kapitaniak, *Nonlinear Dynamical Systems With Self-Excited and Hidden Attractors*. Berlin, Germany: Springer, 2018.
[31] N. Sharma, P. Kumar, and S. K. Rai, "A new approach to implement stream cipher using memristor-based Chua's circuit for secure communication," *AEU-Int. J. Electron. Commun.*, vol. 175, Feb. 2024, Art. no. 155105.
[32] A. O. Adelakun and S. T. Ogunjo, "Active control and electronic simulation of a novel fractional order chaotic jerk system," *Commun. Nonlinear Sci. Numer. Simul.*, vol. 130, Mar. 2024, Art. no. 107734.
[33] A. A.-H. Shoreh and G. M. Mahmoud, "A novel adaptive synchronization algorithm for a general class of fractional-order complex-valued systems with unknown parameters, and applications to circuit realization and color image encryption," *Phys. Scripta*, vol. 99, no. 2, Feb. 2024, Art. no. 025212.
[34] D. Shah, T. Shah, I. Ahamad, M. I. Haider, and I. Khalid, "A three-dimensional chaotic map and their applications to digital audio security," *Multimedia Tools Appl.*, vol. 80, no. 14, pp. 22251–22273, Jun. 2021.
[35] W. Dai, X. Xu, X. Song, and G. Li, "Audio encryption algorithm based on Chen memristor chaotic system," *Symmetry*, vol. 14, no. 1, p. 17, Dec. 2021.
[36] P. K. Naskar, S. Bhattacharyya, and A. Chaudhuri, "An audio encryption based on distinct key blocks along with PWLCM and ECA," *Nonlinear Dyn.*, vol. 103, no. 2, pp. 2019–2042, Jan. 2021.
[37] S. Adhikari and S. Karforma, "A novel audio encryption method using Henon–Tent chaotic pseudo random number sequence," *Int. J. Inf. Technol.*, vol. 13, no. 4, pp. 1463–1471, Aug. 2021.

TALAL BONNY received the M.Sc. degree from the Technical University of Braunschweig, Germany, in 2002, and the Ph.D. degree from Karlsruhe Institute of Technology, Germany, in 2009. He is currently an Associate Professor with the Department of Computer Engineering, College of Computing and Informatics, University of Sharjah, where he has been a Faculty Member, since 2013. His current research interests include embedded systems, hardware digital design, image processing, chaotic oscillator realizations, secure communication systems, AI and machine learning, and bioinformatics. He served as a reviewer/a TPC member in many IEEE/ACM journals/conferences. He was the Session Chair of the IEEE Conference on Advances in Artificial Intelligence.

SUNDARAPANDIAN VAIDYANATHAN received the Doctor of Science degree in electrical and systems engineering from Washington University, St. Louis, MO, USA, in May 1996. He is currently a Professor and the Dean of the Centre for Control Systems, Vel Tech University, Avadi, Chennai, India. He is also a Distinguished Visiting Professor with the Centre of Excellence for Research, Value Innovation and Entrepreneurship (CERVIE), UCSI University, Kuala Lumpur, Malaysia. He has published more than 600 Scopus-indexed research publications. His current research interests include linear and nonlinear control systems, chaotic and hyperchaotic systems, circuits, intelligent control, optimal control, mathematical modeling, and scientific computing.

WAFAA AL NASSAN received the bachelor's degree in electronic engineering from the University of Aleppo, Syria, in 2013. Currently, she is a Research Assistant with the University of Sharjah. Her current research interests include modeling and simulating dynamical systems, control systems, embedded systems, information security, machine vision, and intelligent robotics.

FAREH HANNACHI received the Ph.D. degree in applied mathematics from the University of Oum El Bouaghi, Algeria, in 2018. He is currently an Associate Professor with Echahid Cheikh Larbi Tebessi University, Tebessa. His research interests include dynamical systems, chaos, synchronization, mathematical modeling and control systems, and topics related with applied mathematics.

ACENG SAMBAS received the Ph.D. degree in mathematics from Universiti Sultan Zainal Abidin (UniSZA), Malaysia, in 2020. He has been a Lecturer with UniSZA, and the Muhammadiyah University of Tasikmalaya, Indonesia. His current research interests include dynamic systems, chaotic signals, electrical engineering, computational science, signal processing, robotics, embedded systems, and artificial intelligence.